Published in final edited form as:
J Neurophysiol. 2007 June ; 97(6): 4162–4172.

Action potential timing precision in dorsal cochlear nucleus pyramidal cells

Sarah E. Street[1] and **Paul B. Manis**[1,2]

1*Department of Cell and Molecular Physiology University of North Carolina Chapel Hill Chapel Hill, NC 27599*

2*Department of Otolaryngology/Head and Neck Surgery University of North Carolina Chapel Hill Chapel Hill, NC 27599*

Abstract

Many studies of the dorsal cochlear nucleus (DCN) have focused on the representation of acoustic stimuli in terms of average firing rate. However, recent studies have emphasized the role of spike timing in information encoding. We sought to ascertain whether DCN pyramidal cells might employ similar strategies and to what extent intrinsic excitability regulates spike timing. Gaussian distributed low-pass noise current was injected into pyramidal cells in a brain slice preparation. The shuffled auto-correlation-based analysis was used to compute a correlation index of spike times across trials. The noise causes the cells to fire with temporal precision (standard deviation ≅ 1-2 msec) and high reproducibility. Increasing the coefficient of variation of the noise improved the reproducibility of the spike trains, whereas increasing the firing rate of the neuron decreased the neurons' ability to respond with predictable patterns of spikes. Simulated IPSPs superimposed on the noise stimulus enhanced spike timing for > 300 msec, although the enhancement was greatest during the first 100 msec. We also found that populations of pyramidal neurons respond to the same noise stimuli with correlated spike trains, suggesting that ensembles of neurons in the DCN receiving shared input can fire with similar timing. These results support the hypothesis that spike timing can be an important aspect of information coding in the DCN.

Keywords

auditory system; hearing; cochlear nucleus; spike timing; inhibition; synchrony; potassium channels

Introduction

Spike timing and average spike rate are both considered elements of the neural code that represents information about the sensory environment. While neurons can communicate using average rate (Shadlen and Newsome 1998), precise and reproducible spike timing is also frequently observed, raising the likelihood that this firing regime is used to encode information (Abeles et al. 1993; Bair and Koch 1996; Beierholm et al. 2001; Berry et al. 1997; Buonomano 2003; Buracas et al. 1998; de Ruyter van Steveninck et al. 1997; Mainen and Sejnowski 1995; Nowak et al. 1997; Reich et al. 1997). The precision and reliability of action potential timing depends upon the membrane time constant, fluctuations in both excitatory and inhibitory input, the activation of, and noise from, voltage-gated ion channels, and coincident excitation from pre-synaptic neurons (Azouz and Gray 2000; Diesmann et al. 1999; Dorval and White

Corresponding Author: Paul B. Manis, Ph.D. Dept. of Otolaryngology/Head and Neck Surgery 1123 Bioinformatics Bldg., CB#7070 130 Mason Farm Road Univ. of North Carolina at Chapel Hill Chapel Hill, NC 27599-7070 Tel: (919) 966-8926 Fax: (919) 966-7656 email: pmanis@med.unc.edu.

2005; Fricker and Miles 2000; Gauck and Jaeger 2003; 2000; Grande et al. 2004; Grothe and Sanes 1994; Hausser and Clark 1997; Jaeger and Bower 1999; Schreiber et al. 2004; Sourdet et al. 2003; Svirskis et al. 2003; Svirskis et al. 2002; 2004). Certain neurons in the auditory system have long been known to represent precisely timed information about the acoustic environment by phase-locking in their spike trains (Rose et al. 1967), and this depends on specific combinations of ion channels and synaptic receptors. However, many other auditory nuclei, such as the dorsal cochlear nucleus (DCN), show little high-frequency phase-locking and so have been most extensively characterized in terms of mean firing rate.

Pyramidal cells in the DCN receive auditory information via the auditory nerve, and non-auditory information that is relayed through a system of granule cells that give rise to parallel fibers, similar to the circuitry found in the cerebellum. Pyramidal cells integrate synaptic input from these excitatory inputs, as well as from at least three types of inhibitory interneurons, and pass this processed information on to the inferior colliculus (for review, see (Oertel and Young 2004)). While the DCN has not previously been thought to utilize precise spike timing because it exhibits poor phase locking to high-frequency, pure tones (Goldberg and Brownell 1973; Rhode and Smith 1986), recent evidence suggests that timing might play an important role in information processing. For example, parallel fiber synapses onto pyramidal cells exhibit spike timing dependent plasticity (Tzounopoulos et al. 2004). The EPSP-spike coincidence window for plasticity in the DCN is on the order of 10 msec, which is notably smaller than the window reported for other regions of the brain. Furthermore, pyramidal cells exhibit sensitivity to temporal information by encoding the envelope of amplitude modulated sounds up to a few hundred Hz (Frisina et al. 1994; Joris and Smith 1998; Kim et al. 1990; Neuert et al. 2005; Zhao and Liang 1995). Together, these observations support the hypothesis that spike timing may be an important code in this nucleus.

Since spike timing may be important in DCN information coding, we sought to characterize the ability of pyramidal cells of the DCN to respond to time-varying stimuli with reproducible spike trains *in vitro,* and to identify features of the stimulus that affect spike timing. Using Gaussian distributed noise current pulses, to simulate fluctuations in synaptic drive, we were able to determine if time-varying input improves the reproducibility of spike times. The results indicate that pyramidal cells can fire with good precision in response to dynamic stimuli and that firing precision can be affected for several hundred milliseconds by brief hyperpolarizations.

Materials and Methods

Slice Preparation

Sprague-Dawley rats, post-natal day 10-14, and 21-24 were deeply anesthetized with ketamine (100 mg/kg),-xylazine (10 mg/kg) , decapitated, and the brainstem removed. The brainstem was trimmed to a block of tissue that included the dorsal cochlear nucleus. The block was mounted on agar supports, sliced in the transstrial plane (250μm) (Blackstad et al. 1984), and stored in an incubation chamber for 1-2 hours at 34°C. All procedures were performed under protocols approved by the Institutional Animal Care and Use Committee of the University of North Carolina. Slices were transferred to the recording chamber, held in place by a net, and perfused with recording solution at 34°C at 3-5mL/min.

Solutions

The dissection and slicing procedure was carried out in a low Ca^{2+}/high Mg^{2+} solution, which contained the following (in mM), 122 NaCl, 3 KCl, 1.25 KH_2PO_4, 25 $NaHCO_3$, 20 glucose, 2 myo-inositol, 2 sodium pyruvate, 0.4 ascorbic acid, 0.1 $CaCl_2$, and 3.7 $MgSO_4$. The slices were incubated and perfused with the same solution, except containing (in mM) 2.5 $CaCl_2$ and

1.2 $MgSO_4$. Solutions were continuously equilibrated with 95%/5% O_2/CO_2 at 34° to maintain pH at 7.3-7.4, and the osmolarity ranged from 310-320 mOsm. Strychnine (2μM) was added to the bath to block glycinergic inhibition in all experiments. In some experiments, ZD7288 (20μM) was used to block hyperpolarizing-activated channels (BoSmith et al. 1993). The electrode solution contained the following (in mM), 4 NaCl, 130 potassium gluconate, 0.2 EGTA, 10 HEPES, 2 Mg_2ATP, $2Mg_2GTP$, and 2 creatine phosphate. AlexaFluor 488 (Na^+ Salt, Molecular Probes, Eugene, OR) was added to the electrode solution (0.1 mM) allowing cells to be visualized and characterized morphologically. All chemicals were obtained from Sigma-Aldrich (St. Louis, MO) with the exception of ZD7288, which was obtained from Tocris Bioscience (Ellisville, MO).

Recording

Electrodes were pulled from 1.5 mm diameter KG-33 glass (Garner Glass, Claremont, CA) to a tip diameter of 1-2 μm and a final tip resistance of 2-7 MΩ on a P-2000 Sutter puller. The tips were coated with Sylgard 184 (Dow Corning, Midland, MI) to decrease pipette capacitance. The slices were transferred to the recording chamber on a fixed stage microscope and visualized with a 40X, 0.75 NA or 63X 0.9 NA water immersion objectives using video-enhanced differential interference contrast illumination in infrared light. Pyramidal cells were selected based on shape and visualization of apical and basal dendrites at opposite ends of the cell body. The membrane potential was recorded using standard techniques for whole-cell, tight seal recording in slices with a Multiclamp 700A amplifier (Molecular Devices, Foster City, CA). Data acquisition was carried out under computer control with custom software program written in Matlab (The Mathworks, Natick, MA) using high-speed 12 or 16 bit A-D boards (National Instruments, Austin, TX) with a sampling rate of 50 kHz. All voltages were corrected for a −12 mV electrode-bath junction potential during analysis.

Stimuli

Different types of stimuli were applied to the pyramidal cells. The first was a rectangular DC current pulse, shaped using $\cos^2$ramps to minimize onset and offset transients. The other was a low-pass (250-1500 Hz) filtered (8-pole Butterworth digital filter) noise current (peak to peak amplitude of 500 pA unless otherwise noted).

The exact amplitude and pattern of synaptic input that pyramidal cells receive is currently unknown. While some *in vivo* measurements of membrane potential fluctuations have been made, these measurements probably do not accurately reflect the frequency content of the membrane potential nor the relevant amplitudes of the fluctuating and steady-state components due to the low-pass filtering effect of sharp electrodes. Therefore we chose a Gaussian noise waveform, which theoretically includes all possible combinations of current trajectories that a cell might encounter. However, only a limited range of frequency content and amplitudes are biologically plausible, so our stimulus waveform was selected so as to present an experimentally tractable part of this large parameter space.

There are a number of factors that were considered in the selection of the input noise. In the present experiments, current is injected into the cell body in order to manipulate the membrane potential and drive the spike generator. Since this current is injected close to the spike generator, the membrane potential fluctuations should resemble those that would be seen by the spike generator when driven by both distant synaptic inputs that have been filtered by dendrites, and by proximal excitatory and inhibitory conductances. Consequently, excitatory events will be low pass-filtered by the transfer function between the dendrites and the cell body. However, this transfer function varies for each synapse, and therefore the aggregate effect of ongoing synaptic input necessarily generates synaptic potentials with a range of rise times and amplitudes. Experimental measures from other cochlear nucleus cells with membrane time

constants similar to pyramidal cells suggest that during excitatory auditory drive, the spike generation site will experience both a slow sustained membrane depolarization, and superimposed rapid fluctuations that are low pass filtered (~200 Hz) version of the synaptic input (White et al. 1994). High-frequency barrages of both excitatory input from the auditory nerve and inhibitory input of the vertical cells can exceed 300 Hz from single inputs. Synaptic conductances from excitatory synapses onto DCN pyramidal cells have a rise-time (10-90%) of 430 microseconds, and decay time constants averaging 1.3 msec (Gardner et al. 2001). For inhibitory inputs that occur close to the cell body, dendritic filtering is less important, and the voltage trajectory is determined instead by the time course of the synaptic conductance and by the somatic membrane time constant. IPSCs onto pyramidal cells have rise times of 2-4 msec, and decay time constants of 5-10 msec (Mancilla and Manis, unpublished observations). To estimate the spectral content produced by these synaptic inputs, we represented the conductance waveforms with an alpha function and calculated the energy spectrum of the conductance change. These calculations revealed that most of the time-averaged the energy is at 200 Hz and below for single events (tau = 2 for an alpha function for the EPSCs); however during the rising phase of the EPSCs, there is energy at frequencies approaching 1 kHz. The membrane potential may follow such rapid changes if the cell is an active state (e.g., high conductance state due to synaptic activity). We therefore expect to see frequency content in the membrane potential that includes both lower frequency components representing the time course of the EPSC and the rate of individual synaptic inputs, and components perhaps as high as 1 kHz representing rapid changes in the membrane potential during the rising phase of the EPSCs. Taken together, these considerations suggest that an appropriate stimulus to test the cell's temporal coding abilities should include a broad range of frequencies, up to about 1 kHz.

The Gaussian noise was superimposed on the DC pedestal. Adjusting the amplitude of the DC pedestal controlled the average firing rate of the cell. Experiments examining spike timing used frozen noise in which the same noise token was used for 100 consecutive trials. To determine the spike triggered average of the cells, random noise was generated by changing the noise token in each trial for 50 consecutive trials. A simulated IPSP (sIPSP) or simulated EPSP (sEPSP) consisting of a short train of three alpha waves [$I(t) = I_{max}*\alpha*t* \exp(-\alpha*t)$; $\alpha=0.1$ $msec^{-1}$], separated by a 15 msec interevent interval, was added to the stimulus with a delay of 500 msec, allowing us to compare the regularity of firing before and after the sIPSP or sEPSP. The sIPSP and sEPSP amplitudes were visually estimated from averaged traces, using a cursor. Since the sEPSPs evoked spikes, the measurements were made on the largest events that preceded spikes, or that were visible as inflections at the initiation of the spike. sIPSPs were 11.4 +/− 3.4mV for 18 cells, while sEPSPs were 4.8 +/− 1.5 mV in the same cells. The sEPSPs are smaller than the sIPSPS even though the same current was used for each set of events. The differences arises because the cells were close to spike threshold, so the measurements are an underestimate of the true amplitude because the sEPSPs were partly obscured by the spikes, and also because the cells were depolarized and had a low input resistance at the time the sEPSPs were delivered, which reduces the amplitude of the voltage deflection. Previously published measurements of membrane hyperpolarizations were reported to be 5-9 mV (Hancock and Voigt 2002; Rhode et al. 1983)

Analysis

The digitized current and voltage traces were stored in a Matlab file and were then analyzed using custom Matlab routines. To determine the reproducibility of spike trains, we used the shuffled autocorrelogram (SAC) method first described by Joris (Joris 2003; Joris et al. 2006; Louage et al. 2004). For each cell, all non-identical spike trains were paired with each other and the forward time intervals between all spikes of each spike train were used to calculate a cross correlation of the delay between spike times. This histogram is referred to as the SAC. The SAC was normalized by dividing the number of coincidences in each bin (0.1 msec wide)

by $N(N-1)r^2\Delta\tau D$, where N is the number of presentations (100), r is the average firing rate, $\Delta\tau$ is the choice of bin width and D is the duration of the stimulus (note that the result is dimensionless). We then fit the normalized value to a Gaussian function to measure the width of the central correlation peak. The height of the Gaussian at 0 delay, the correlation index, (CI; see (Joris et al. 2006)) can then be used to compare the spike timing in response to different stimuli. Since this method is sensitive to changes in mean spike rate during the collection of repeated trials, we used a selection criterion to identify stable recording epochs for comparison. The slope of the firing rate as a function of time was calculated. Any cell that had a mean rate that changed by more than 2 spikes per 1-second trial was discarded. This selection criterion was specifically used for experiments that compared the CI for stimuli that included the sIPSP and the sEPSP. The SAC method does not require *a priori* knowledge of the correlation structure, and thus provides an objective measure of spike timing across trials.

We also calculated the reverse correlation, or spike triggered average (STA) of the current waveform that elicited an action potential. In these experiments we presented the cell with 50 independent noise tokens and then computed the STA for spikes whose preceding ISI was greater than 25 msec. Confidence intervals were calculated according to Bryant and Segundo (1976).

Data analysis was performed with Matlab 7.1 and Igor Pro (5.04). Statistics were calculated using both Matlab 7.1 and Prism 3.0 (GraphPad Software, San Diego, CA). All numerical data are presented as means ± standard deviation (SD). Statistical tests of hypotheses used one or two-sided, paired or unpaired (as appropriate) t-tests.

Results

Responses of Pyramidal Cells to a White Noise Current Injection

We first sought to determine whether pyramidal cells of the DCN are capable of firing reliable and precise trains of action potentials. A total of 45 pyramidal cells with a mean resting membrane potential of –63.1 ± 4.9 mV and a mean input resistance of 68.2 ± 38.4 MΩ were identified and recorded for the initial experiments. All cells showed the typical response patterns to depolarizing current pulses including regular, non-adapting trains of spikes, pauser and build-up patterns (Manis 1990). Seventeen cells were confirmed to be pyramidal cells morphologically. We do not include any cells that show bursting action potentials (likely cartwheel cells) in these results.

We tested whether cells were sensitive to the temporal structure of the membrane potential by comparing responses to a flat depolarizing current pulse with responses to stimuli with a superimposed noise. The DC current was chosen so that the cell fired at 20 ± 5 Hz. In response to the DC current (Figure 1A), the cells typically respond with a train of action potentials with regular interspike intervals (ISI). The precise timing of spikes varied between trials. One can easily observe this behavior by examining a raster plot of spike times (Figure 1B). The precision of the spike times in response to a flat current injected is high at the beginning of the spike train, but decreases as the stimulus continues.

In contrast, when low-pass filtered (500Hz) Gaussian noise is superimposed on the DC pedestal (Figure 1D), the cell tends to fire spikes at specific times during the stimulus, forming discernable spike time “events” that are visible in the raster plot (Figure 1E). The precision of the spike times from the noise current was high throughout the duration of the stimulus. This is also visible in the raster plot and the PSTH (Figure 1 E, F).

To calculate the repeatability of the spike trains we used the SAC analysis (see methods). The SAC reports both reliability (by the CI) and the precision (by the SD of the Gaussian function).

The SAC uses the difference in spike times between pairs of different trials from the same cell to reveal repeatable temporal structure in the spike train. In response to the flat current pulse, the spike delays are spread out broadly, and have a mean value of 1 (Figure 2A). This flat SAC indicates that there is no repeated spike timing structure across trials. However, in response to the noisy current, the delays between spike times in different trials are frequently small, and the SAC shows a large peak around zero delay. The peak can be reasonably fit with a Gaussian function (shown by the line in Figure 2A). Across the population of cells, noisy current pulses elicit higher central peaks than flat currents (Figure 2B). While our recordings were done in P10-P14 animals, the same result was seen in 5 cells from P20-P24 animals where the peripheral auditory system is fully developed ($P<0.01$, mean difference of CI between each pair=12.07, mean difference of precision in each pair was 19.28 msec, $P<0.0001$).

Sensitivity of SAC to Spectral Structure of the Noise Input

Pyramidal cells of the DCN have been shown to phase lock to auditory input at low frequencies, and they can encode the frequency and amplitude modulation of acoustic stimuli up to about 500 Hz (Frisina et al. 1994; Kim et al. 1990; Rhode and Greenberg 1994; Zhao and Liang 1995). These observations led us to investigate how the frequency content of the noise current stimulus affected the ability of the pyramidal cells to fire in a repeatable manner. We varied the low-pass cutoff between 250 to 1750 Hz. Varying the noise spectrum did not alter the ability of the cells to respond reliably to the noise (Figure 3); although the CI values were variable across cells, there was little evidence for any frequency-dependence. Consequently, we choose to use a low-pass filter frequency of 500 Hz for our subsequent analyses.

Dependence of CI on Firing Rate

It is expected that the reliability might depend on the mean firing rate of a cell. At high firing rates, spike generation is dominated by intrinsic conductances, whereas at low rates, the variability of the membrane potential due to synaptic input or noise is expected to play a larger role. We thus calculated the CI for pyramidal cells firing at low, medium and high rates to a noisy current. The firing rate was manipulated by increasing the DC pedestal on which the noise is superimposed, without increasing the amplitude of the noise itself. In general, the faster the average firing rate, the weaker the correlation between spike times across trials with the same stimulus presented (Figure 4A,B). However, note that the precision of spike timing does not change (Figure 4B).

As the DC pedestal is changed, the coefficient of variation of the stimulus (CV_s, measured as the variance divided by the mean amplitude of the stimulus) decreases, and thus co-varies with increasing firing rate. A smaller CV_s could, in part, account for the decrease in reproducibility of the spike trains, since the temporally changing component of the stimulus becomes small relative to the average depolarization. We evaluated the relation between CV_s and the CI (Figure 4C). There is a weak, but significant, positive correlation between CV_s and CI ($P<0.005$, $R=0.341$, $df=63$). To investigate this further, we divided the trials into 3 groups based on the CV of the stimulus, (low, $0.18\leq CV_s<0.28$; intermediate, $0.28\leq CV_s<0.38$; high, CV_s, ≥ 0.38) and plotted spike rate against CI for each group (Figure 4D). Rate was negatively correlated with CI for the intermediate and high CV groups (intermediate: $R=-0.476$, $P=0.017$, $df=22$; high: $R=-0.502$, $P=0.039$, $df=17$), but CI was relatively independent of rate for the low CV group ($R=0.156$, $P=0.52$, $df=19$). Thus, while decreasing the CV_s accounts for part of the decrease in reliability with increasing rate, increasing the rate still results in lower numbers of spike times with small delays in the SAC. Even at the higher rates, spike times are determined by the fluctuations in the noise, since the CI values are all well above 1 (Figure 4D), whereas the CI for flat current pulses is not different from 1. This indicates that, at least for rates up to 100 Hz, the intrinsic mechanisms do not completely govern the spike times.

Since increasing the average firing rate leads to a decreased CI, we next investigated whether increasing the amplitude of the noise improved spike timing reproducibility. Frozen noise tokens with different amplitude, but the same DC pedestal, were presented to the cells for 50 trials (Figure 5A-C). In four out of 5 cells, increasing the noise amplitude results in increased CI of spike times (Figure 5D, E). Since the CV_s increases when the amplitude of the noise component is increased, the time-varying component of the stimulus drives the cell most strongly, and the cell fires in response to the stronger stimulus fluctuations.

Spike Triggered Averages

So far, we have shown that pyramidal cells can respond to time-varying input with reliable and precisely timed spikes. In part, the cells are responding to specific patterns of energy in the stimulus. To identify the time courses of the stimulus events driving the cells, we computed spike-triggered averages by averaging the mean current injected before and after spikes, aligned on spike threshold crossings.

A comparison of STAs is shown in Figure 6 for one cell presented with noise low-pass filtered at 250 Hz (thick line), and noise low-pass filtered at 500 Hz (thin line). The two sets of dashed lines show 95% confidence limits for the two sets of noisy current injections. STAs to flat current pulses had no significant deviations from the baseline current (not shown). However, the STA to both the 250 Hz noise and the 500 Hz low-pass filtered noise reveals a broad negative (hyperpolarizing) followed by a sharp positive (depolarizing) current. The main difference between STAs for the two different spectra is mostly in the high frequency components, but the averages follow a similar time course (Figure 6A). The hyperpolarizing current is small, but lasts for 10 msec, whereas the depolarizing current is large and lasts for only ~3 msec. There is little difference in the rising slope or shape of the action potentials that result from the different input currents (fig. 6B). In most cases, it seems that the cells are more likely to fire an action potential if they experience a slight hyperpolarization immediately before a depolarizing current.

Perturbations in the Stimulus Alter Spike Timing

Inhibition is a critical element of sensory coding in the DCN (Oertel and Young 2004). DCN pyramidal cells receive inhibitory input from at least three different types of interneurons: vertical cells, cartwheel cells and stellate cells. We therefore asked how a simulated IPSP (sIPSP) placed in the middle of the noise stimulus would affect spike timing. We hypothesized that superimposing a sIPSP might increase reliability and precision of subsequent action potentials because the STA suggests that these cells prefer to fire when a small hyperpolarizing current precedes a depolarizing current. A sIPSP, consisting of a rapid triplet of alpha waves, was superimposed on the Gaussian noise current 500 msec after the onset of the stimulus (Figure 7A,B). We then compare the SACs after the sIPSP.

The SACs revealed that the spike times were more highly correlated after the sIPSP (Figure 7C). However, the sIPSP briefly hyperpolarizes the cells, and prevents the noise current from triggering action potentials. After the sIPSP, the first spike is more precise and reliable. The effect continues for at least 300 msec (Figure 7B). Summary data for 28 cells is shown in Figure 7D-E. For the last 500 msec of the stimulus, the CI is higher when the stimuli contain a sIPSP. The CI of spike times that occur before the sIPSP is similar to that under control conditions indicating that the sIPSP is not affecting the CI at these times. The difference in the CI after a sIPSP is highly significant ($P<0.001$; $N=31$, paired t-test). In order to determine approximately how long the sIPSP affected the spike times, we compared the CI's of smaller time intervals using a sliding time scale of 100 msec (Figure 7E). In the five 100 msec time intervals prior to the sIPSP, there is no difference in CI. However, the CI of the 100 msec interval that includes the spikes from the 450 msec time point to the 550 msec time point (point a in figure 7E) was

significantly higher compared to the same time interval without an sIPSP (P=0.0003, df=25, mean difference=−2.088). The effect continued for the next two 100 msec intervals (see points b and c, Figure 7E). The CI's for the 550-650 msec interval and 650-750 msec interval were both higher when an sIPSP was present in the stimulus compared to when there was no sIPSP, although the effect was not as pronounced as the 450-550 msec interval (b. P=0.022, DF=32, mean difference=−0.404, c. P=0.0104, DF=32, mean difference=−0.204).

Following the sIPSP, the increase in synchrony could result from the hyperpolarization of the membrane potential, or it could result from any perturbation. We tested the second idea by presenting the frozen noise stimuli superimposed with a sEPSP (Figure 8A). The sEPSP produced a brief increase in spike rate, followed by a small hyperpolarization and a delay to the next spike. Spike timing following the sEPSP is more reliable and precise than it would have been without the sEPSP (Figure 8B,C), although the increase in CI is not as pronounced with the sEPSP as with the sIPSP (P<0.05, N=10, paired t-test). While cells fire up to 3 action potentials during the sEPSP, there also is a slight after-hyperpolarization might effectively recruit the same mechanisms as the sIPSP. We also used the sliding time window analysis to determine how long the effects of the sEPSP lasted. However, the there were no statistically different intervals either before or after the sEPSP (Figure 8D). Therefore, we conclude that a sEPSP is not as effective as a sIPSP in improving the spike timing. In conclusion, small perturbations of the membrane potential, such as a sIPSP, can affect the CI for several hundred msec, and it is most likely that the membrane hyperpolarization engages additional mechanisms that affect subsequent spike timing.

Population coding

The data shown so far suggest that individual cells can respond with repeatable patterns of activity in response to a frozen stimulus waveform. However, temporal coding also requires the coordinated activity of many neurons at the same time, for example. Since each neuron has different intrinsic excitability due to the differences in the voltage-dependence and density of their ion channels (for example, see (Kanold and Manis 2001; 2005)), such a temporal code might not be effectively retained across a population of cells receiving similar inputs. To investigate whether synchronous firing can be generated by a common stimulus to a population of cells, we computed the SAC, as a measure of synchrony, across a population of 15 cells collected in 6 independent experiments over a 2-month period, where the same noise token was used for each cell. Such a calculation provides an estimate of the coherent firing that is available across the population of cells. On average, the frozen noise generated a population SAC with a similar shape to that seen in individual cells (Figure 9A). The synchrony was good (CI=4) and the timing of correlated spikes had a half-width of 0.84 msec. The amplitude of the central peak was smaller than for individual cells, indicating that fewer spikes were correlated between cells than within a single cell. A small secondary peak with a 2-msec half-width also appeared (arrow in Figure 9A), suggesting that the spike timing across the population was not quite as temporally precise as in individual cells. The flat current pulse did not result in an elevated central SAC peak, in spite of the regular discharge of all cells. The SAC had the same shape and amplitude even in single trials (Figure 9B), raising the possibility that the synchronized firing could convey information about the stimulus with good temporal precision during a single stimulus.

We next examined the synchronization between individual cells by calculating the cross-correlation of spike trains. The peak correlations for both noisy and flat current stimuli are summarized across the 105 possible pair-wise comparisons for the 15 cells in this population in Figure 9C. Flat pulses (black line) result in low peak correlation rates that are not significantly different from those obtained with noisy stimuli when one of the spike trains is shuffled to remove temporal correlations (not shown). The noise correlations however show a broad

distribution: some cell pairs exhibit relatively high correlations, whereas other pairs show little correlation. Overall, however, the correlated firing rate is at least 2.7 times higher with the noise than with flat pulses. The correlated rate with flat pulses is probably lower than what we estimate, since we chose the maximum correlation value, which is influenced by the statistical variation in the cross-correlation function due to the finite number of spikes available for the computation. Thus, common features in the stimulus can lead to correlated firing among different cells, and the correlations occur in a time window about 2 msec wide.

Discussion

We have shown that DCN pyramidal cells *in vitro* can respond to time-varying stimuli with reliable and precise trains of action potentials. The SAC (Joris 2003; Joris et al. 2006; Louage et al. 2004), a method that is free of assumptions regarding the timing of spikes in relationship to stimulus events, reveals that pyramidal cells can reliably report temporal events in a stimulus with millisecond precision. Precise spike timing can even be seen across a population of cells with different intrinsic properties. Characteristics of the stimulus such as amplitude and variability alter the reliability of the output spike train, whereas the degree of low-pass filtering does not affect the reliability. Longer hyperpolarizing events, such as a sIPSP embedded in the stimulus, can increase the reliability and precision of firing for up to 300 msec.

General Characteristics of DCN Pyramidal Cells in Response to Noise

Many neurons in the auditory system are known for their ability to fire action potentials that occur in a precise temporal relationship to the stimulus (Carr et al. 2001; Oertel 1999; Trussell 1999). Such cells may fire on repeated portions of the waveform with a standard deviation on the order of 115 μsec (corresponding to a phase-locking vector strength of 0.8 at 1 kHz); these cells have specialized AMPA receptor subunit and synaptic configurations, and express low-voltage activated potassium conductances. Such specializations are not present in DCN pyramidal cells (Hirsch and Oertel 1988; Kanold and Manis 1999; Manis 1990; Zhang and Oertel 1994), so it expected that DCN cells respond similarly to other “generic” neuronal types when presented with time-varying input that resembles synaptic input (de Ruyter van Steveninck et al. 1997; Mainen and Sejnowski 1995; Nowak et al. 1997). The STA current waveform, which represents the linear contribution of current to spike generation, has a relatively short time scale in DCN pyramidal cells as compared to neocortical neurons. The spike-triggered average current waveform consisted of a small slow hyperpolarizing current followed by a rapidly rising depolarizing current as in other cells. However, in other cells the hyperpolarizing and fast depolarizing phases of the current have been reported to last tens of milliseconds (Mainen and Sejnowski 1995). In DCN pyramidal cells the hyperpolarizing phase lasted about 10 msec, and the depolarization on average had a half-width of 3 msec. This suggests that DCN pyramidal cells should integrate synaptic conductances on a relatively short time scale. The sharp depolarization most effectively enables the cell to reach threshold, because the spike threshold is inversely proportional to the slope of the input current (Azouz and Gray 2000). Thus, fast events in the stimulus not only lead to sharp membrane depolarizations, but also decrease the threshold resulting in an increased probability of firing a spike. Pyramidal cells thus appear to integrate their inputs on a time scale that is between that of the specialized auditory neurons that show high-frequency phase locking, and the slower neurons of the forebrain. On the other hand, DCN pyramidal cells also have a temporally non-linear set of membrane conductance changes that can influence spike timing well beyond the 10 msec window suggested by the STA (Figure 7, also see Kanold and Manis, 1999, 2001, and Manis et al., 2003).

When we increased the variance in the stimulus (increased $CV_{s,}$), spike times became more reproducible. The higher amplitudes of the time-varying component increase the magnitude

of depolarizing currents. The faster and larger membrane depolarizations permit less time for intrinsic conductances of the cell to oppose the depolarization, and less time for Na^+ channels to inactivate. These two features lead to a lower spike threshold and higher reliability and precision (Hunter and Milton 2003).

The variance of the synaptic input to DCN pyramidal cells *in vivo* has not been measured. However, even small variations in the input current can evoke reliable spike trains when the stimulus frequency resonates with the intrinsic cell membrane oscillations or with a characteristic firing frequency (Fellous et al. 2001; Haas and White 2002; Hunter et al. 1998). We also found that small increases in noise amplitude resulted in increases in the number of spikes that were tightly correlated across trials. DCN pyramidal cells exhibit subthreshold oscillations that range in frequency from 40 to 100 Hz (Manis et al. 2003). While we did not explore small amplitude stimuli that specifically incorporated enhanced energy within this frequency range, it is possible that these cells could increase their firing reliability when the input resonates with membrane dynamics.

We compared neurons that fired at the same average rates to determine if pyramidal cells fire more reliable trains of action potentials in response to temporally changing input. While pyramidal cells have been reported to phase lock *in vivo* to low-frequency input, at higher frequencies this phenomenon disappears (Rhode and Smith 1986). In addition others have reported that DCN cells phase lock poorly to synchronized repetitive stimulation of the ANFs (Babalian et al. 2003). As the firing rate of a neuron increases, the ISI is less influenced by transient changes in membrane potential and is controlled to a greater extent by the ionic conductances that regulate the refractory period. Consistent with this, when cells were sorted according to the stimulus CV_s, the precision of spike times decreased with increasing rate. However, the peak rate of the SAC, regardless of CV_s and rate, is very high compared to stimuli that contain no temporal structure. The CI of the ANF SACs runs in the range 2-10, even for stimuli that produce strong phase locking (Louage et al. 2004); the temporal coding in DCN cells can easily achieve this same range though with less precision. While reliability and precision decreases with increasing firing rate, the rates must be well above 100 Hz before the contribution of input current fluctuations ceases to be evident in the spike timing.

Inhibition and Spike Timing in the DCN

Inhibition's effect on spike timing has received immense attention in recent years. In both the cerebellum and the medial superior olive, inhibition masks integrated, sub-threshold input which results in the cell failing to fire when the input is weak; instead the cell only responds to stronger, coincident synaptic events that elicit more reliable spikes (Gauck and Jaeger 2000; Grothe and Sanes 1994). Inhibition also leads to a delay in spike times in the cerebellum and DCN (Hausser and Clark 1997; Kanold and Manis 2005), while it shortens the membrane time constant and increases the membrane conductance. Consequently, non-synchronous EPSPs become smaller and briefer, allowing the neuron to act as a more precise coincidence detector (Grande et al. 2004; Jaeger and Bower 1999). The DCN contains at least three types of inhibitory interneurons that share excitatory input with pyramidal cells (Golding and Oertel 1997; Hackney et al. 1990; Oertel and Young 2004). These interneurons can strongly inhibit pyramidal cells in conjunction with activity in ANFs and parallel fibers. Since inhibition is prominent in this nucleus, we imposed a sIPSP to mimic the inhibitory input from the bursting cartwheel cells. This perturbation transiently silenced the cell firing, but resulted in an increased precision of spike timing when the cell resumed activity. The hyperpolarization from the sIPSP most likely perturbs the state of the cell's intrinsic conductances, such as sodium channels and transient potassium currents, and puts the cell membrane into a regime where it is can reliably fire at the next sharp depolarization. Cartwheel cells and stellate cells, both of which receive input from parallel fibers, could provide synchronized inhibitory input to pyramidal cells after

they are excited by the parallel fibers. This inhibition might prevent pyramidal cells from firing imprecisely-timed spikes to small depolarizing events after the initial excitation from the parallel fibers. This inhibition could also deinactivate membrane conductances so that the cells would be prepared to fire at the next sharp depolarization).

Population coding

A surprising result was that correlated spike times could be measured in a population of cells from different animals and slices, in response to the same stimulus. This suggests that a population of pyramidal cells could use a timing-based, population-coding scheme to represent auditory information (Kanold and Manis 2005). This hypothesis depends on two principal assumptions. First it is assumed that the firing of individual auditory nerve fibers that connect to a group of pyramidal cells shows stimulus-dependent correlations in their firing. Indirect evidence suggests that this is the case, even for high-CF auditory nerve fibers. Responses to repeated stimuli in individual fibers show a significant central peak in their SAC (Louage et al. 2004). In addition, these correlations need to be detected by the pyramidal cells, and the presence of stimulus-dependent central mounds in the cross-correlations of pyramidal cells suggests that this may occur (Voigt and Young 1988). Second, this hypothesis assumes that the pyramidal cells receiving common inputs converge onto individual neurons in the inferior colliculus in a way that allows the collicular neurons to respond to the correlations in the input; this assumption is necessary for correlated synaptic events across the cell population to be detected and operated on. The convergence patterns between pyramidal cells and their collicular targets are presently not well understood.

Recent studies have demonstrated the existence of long-term synaptic plasticity between parallel fibers and two target neurons in the DCN, the pyramidal and the cartwheel cells (Fujino and Oertel 2003; Tzounopoulos et al. 2004). The timing-dependence of this plasticity is relatively precise: in the pyramidal cells the window is less than 20 milliseconds wide and in cartwheel cells it is less than 5 msec wide. Such a narrow window demands that the firing of the postsynaptic cells to fluctuating synaptic inputs also be temporally precise, and implies that precise spike timing is an integral part of information processing in the DCN, at least as it relates to long-term synaptic plasticity. Our results also demonstrate that precise spike timing can occur in response to dynamic stimulation, and that interactions between inhibition, potassium conductances, and other conductances regulating intrinsic cell excitability can modulate the precision of spike timing over hundreds of milliseconds.

Acknowledgements

This work was supported by grants from NIDCD: R01 DC000425 to PBM, and F31 DC07827 to SES. We thank our colleagues for their comments on the manuscript.

References

Abeles M, Bergman H, Margalit E, Vaadia E. Spatiotemporal firing patterns in the frontal cortex of behaving monkeys. Journal of neurophysiology 1993;70:1629–1638. [PubMed: 8283219]

Azouz R, Gray CM. Dynamic spike threshold reveals a mechanism for synaptic coincidence detection in cortical neurons in vivo. Proc Natl Acad Sci U S A 2000;97:8110–8115. [PubMed: 10859358]

Babalian AL, Ryugo DK, Rouiller EM. Discharge properties of identified cochlear nucleus neurons and auditory nerve fibers in response to repetitive electrical stimulation of the auditory nerve. Exp Brain Res 2003;153:452–460. [PubMed: 12955378]

Bair W, Koch C. Temporal precision of spike trains in extrastriate cortex of the behaving macaque monkey. Neural Comput 1996;8:1185–1202. [PubMed: 8768391]

Beierholm U, Nielsen CD, Ryge J, Alstrom P, Kiehn O. Characterization of reliability of spike timing in spinal interneurons during oscillating inputs. Journal of neurophysiology 2001;86:1858–1868. [PubMed: 11600645]

Berry MJ, Warland DK, Meister M. The structure and precision of retinal spike trains. Proc Natl Acad Sci U S A 1997;94:5411–5416. [PubMed: 9144251]

Blackstad TW, Osen KK, Mugnaini E. Pyramidal neurones of the dorsal cochlear nucleus: a Golgi and computer reconstruction study in cat. Neuroscience 1984;13:827–854. [PubMed: 6527780]

BoSmith RE, Briggs I, Sturgess NC. Inhibitory actions of ZENECA ZD7288 on whole-cell hyperpolarization activated inward current (If) in guinea-pig dissociated sinoatrial node cells. Br J Pharmacol 1993;110:343–349. [PubMed: 7693281]

Buonomano DV. Timing of neural responses in cortical organotypic slices. Proc Natl Acad Sci U S A 2003;100:4897–4902. [PubMed: 12668762]

Buracas GT, Zador AM, DeWeese MR, Albright TD. Efficient discrimination of temporal patterns by motion-sensitive neurons in primate visual cortex. Neuron 1998;20:959–969. [PubMed: 9620700]

Carr CE, Soares D, Parameshwaran S, Perney T. Evolution and development of time coding systems. Curr Opin Neurobiol 2001;11:727–733. [PubMed: 11741025]

de Ruyter van Steveninck RR, Lewen GD, Strong SP, Koberle R, Bialek W. Reproducibility and variability in neural spike trains. Science 1997;275:1805–1808. [PubMed: 9065407]

Diesmann M, Gewaltig MO, Aertsen A. Stable propagation of synchronous spiking in cortical neural networks. Nature 1999;402:529–533. [PubMed: 10591212]

Dorval AD Jr. White JA. Channel noise is essential for perithreshold oscillations in entorhinal stellate neurons. J Neurosci 2005;25:10025–10028. [PubMed: 16251451]

Fellous JM, Houweling AR, Modi RH, Rao RP, Tiesinga PH, Sejnowski TJ. Frequency dependence of spike timing reliability in cortical pyramidal cells and interneurons. Journal of neurophysiology 2001;85:1782–1787. [PubMed: 11287500]

Fricker D, Miles R. EPSP amplification and the precision of spike timing in hippocampal neurons. Neuron 2000;28:559–569. [PubMed: 11144364]

Frisina RD, Walton JP, Karcich KJ. Dorsal cochlear nucleus single neurons can enhance temporal processing capabilities in background noise. Exp Brain Res 1994;102:160–164. [PubMed: 7895792]

Fujino K, Oertel D. Bidirectional synaptic plasticity in the cerebellum-like mammalian dorsal cochlear nucleus. Proc Natl Acad Sci U S A 2003;100:265–270. [PubMed: 12486245]

Gardner SM, Trussell LO, Oertel D. Correlation of AMPA receptor subunit composition with synaptic input in the mammalian cochlear nuclei. J Neurosci 2001;21:7428–7437. [PubMed: 11549753]

Gauck V, Jaeger D. The contribution of NMDA and AMPA conductances to the control of spiking in neurons of the deep cerebellar nuclei. J Neurosci 2003;23:8109–8118. [PubMed: 12954873]

Gauck V, Jaeger D. The control of rate and timing of spikes in the deep cerebellar nuclei by inhibition. J Neurosci 2000;20:3006–3016. [PubMed: 10751453]

Goldberg JM, Brownell WE. Discharge characteristics of neurons in anteroventral and dorsal cochlear nuclei of cat. Brain Res 1973;64:35–54. [PubMed: 4360881]

Golding NL, Oertel D. Physiological identification of the targets of cartwheel cells in the dorsal cochlear nucleus. Journal of neurophysiology 1997;78:248–260. [PubMed: 9242277]

Grande LA, Kinney GA, Miracle GL, Spain WJ. Dynamic influences on coincidence detection in neocortical pyramidal neurons. J Neurosci 2004;24:1839–1851. [PubMed: 14985424]

Grothe B, Sanes DH. Synaptic inhibition influences the temporal coding properties of medial superior olivary neurons: an in vitro study. J Neurosci 1994;14:1701–1709. [PubMed: 8126564]

Haas JS, White JA. Frequency selectivity of layer II stellate cells in the medial entorhinal cortex. Journal of neurophysiology 2002;88:2422–2429. [PubMed: 12424283]

Hackney CM, Osen KK, Kolston J. Anatomy of the cochlear nuclear complex of guinea pig. Anat Embryol (Berl) 1990;182:123–149. [PubMed: 2244686]

Hancock KE, Voigt HF. Intracellularly labeled fusiform cells in dorsal cochlear nucleus of the gerbil. II. Comparison of physiology and anatomy. Journal of neurophysiology 2002;87:2520–2530. [PubMed: 11976388]

Hausser M, Clark BA. Tonic synaptic inhibition modulates neuronal output pattern and spatiotemporal synaptic integration. Neuron 1997;19:665–678. [PubMed: 9331356]

Hirsch JA, Oertel D. Intrinsic properties of neurones in the dorsal cochlear nucleus of mice, in vitro. J Physiol 1988;396:535–548. [PubMed: 2457693]

Hunter JD, Milton JG. Amplitude and frequency dependence of spike timing: implications for dynamic regulation. Journal of neurophysiology 2003;90:387–394. [PubMed: 12634276]

Hunter JD, Milton JG, Thomas PJ, Cowan JD. Resonance effect for neural spike time reliability. Journal of neurophysiology 1998;80:1427–1438. [PubMed: 9744950]

Jaeger D, Bower JM. Synaptic control of spiking in cerebellar Purkinje cells: dynamic current clamp based on model conductances. J Neurosci 1999;19:6090–6101. [PubMed: 10407045]

Joris PX. Interaural time sensitivity dominated by cochlea-induced envelope patterns. J Neurosci 2003;23:6345–6350. [PubMed: 12867519]

Joris PX, Louage DH, Cardoen L, van der Heijden M. Correlation index: a new metric to quantify temporal coding. Hear Res 2006;216-217:19–30. [PubMed: 16644160]

Joris PX, Smith PH. Temporal and binaural properties in dorsal cochlear nucleus and its output tract. J Neurosci 1998;18:10157–10170. [PubMed: 9822769]

Kanold PO, Manis PB. A physiologically based model of discharge pattern regulation by transient K+ currents in cochlear nucleus pyramidal cells. Journal of neurophysiology 2001;85:523–538. [PubMed: 11160490]

Kanold PO, Manis PB. Encoding the timing of inhibitory inputs. Journal of neurophysiology 2005;93:2887–2897. [PubMed: 15625095]

Kanold PO, Manis PB. Transient potassium currents regulate the discharge patterns of dorsal cochlear nucleus pyramidal cells. J Neurosci 1999;19:2195–2208. [PubMed: 10066273]

Kim DO, Sirianni JG, Chang SO. Responses of DCN-PVCN neurons and auditory nerve fibers in unanesthetized decerebrate cats to AM and pure tones: analysis with autocorrelation/power-spectrum. Hear Res 1990;45:95–113. [PubMed: 2345121]

Louage DH, van der Heijden M, Joris PX. Temporal properties of responses to broadband noise in the auditory nerve. Journal of neurophysiology 2004;91:2051–2065. [PubMed: 15069097]

Mainen ZF, Sejnowski TJ. Reliability of spike timing in neocortical neurons. Science 1995;268:1503–1506. [PubMed: 7770778]

Manis PB. Membrane properties and discharge characteristics of guinea pig dorsal cochlear nucleus neurons studied in vitro. J Neurosci 1990;10:2338–2351. [PubMed: 2376777]

Manis PB, Molitor SC, Wu H. Subthreshold oscillations generated by TTX-sensitive sodium currents in dorsal cochlear nucleus pyramidal cells. Exp Brain Res 2003;153:443–451. [PubMed: 14508631]

Neuert V, Verhey JL, Winter IM. Temporal representation of the delay of iterated rippled noise in the dorsal cochlear nucleus. Journal of neurophysiology 2005;93:2766–2776. [PubMed: 15846001]

Nowak LG, Sanchez-Vives MV, McCormick DA. Influence of low and high frequency inputs on spike timing in visual cortical neurons. Cereb Cortex 1997;7:487–501. [PubMed: 9276174]

Oertel D. The role of timing in the brain stem auditory nuclei of vertebrates. Annu Rev Physiol 1999;61:497–519. [PubMed: 10099699]

Oertel D, Young ED. What's a cerebellar circuit doing in the auditory system? Trends Neurosci 2004;27:104–110. [PubMed: 15102490]

Reich DS, Victor JD, Knight BW, Ozaki T, Kaplan E. Response variability and timing precision of neuronal spike trains in vivo. Journal of neurophysiology 1997;77:2836–2841. [PubMed: 9163398]

Rhode WS, Greenberg S. Encoding of amplitude modulation in the cochlear nucleus of the cat. Journal of neurophysiology 1994;71:1797–1825. [PubMed: 8064349]

Rhode WS, Oertel D, Smith PH. Physiological response properties of cells labeled intracellularly with horseradish peroxidase in cat ventral cochlear nucleus. The Journal of comparative neurology 1983;213:448–463. [PubMed: 6300200]

Rhode WS, Smith PH. Physiological studies on neurons in the dorsal cochlear nucleus of cat. Journal of neurophysiology 1986;56:287–307. [PubMed: 3760922]

Rose JE, Brugge JF, Anderson DJ, Hind JE. Phase-locked response to low-frequency tones in single auditory nerve fibers of the squirrel monkey. Journal of neurophysiology 1967;30:769–793. [PubMed: 4962851]

Schreiber S, Fellous JM, Tiesinga P, Sejnowski TJ. Influence of ionic conductances on spike timing reliability of cortical neurons for suprathreshold rhythmic inputs. Journal of neurophysiology 2004;91:194–205. [PubMed: 14507985]

Shadlen MN, Newsome WT. The variable discharge of cortical neurons: implications for connectivity, computation, and information coding. J Neurosci 1998;18:3870–3896. [PubMed: 9570816]

Sourdet V, Russier M, Daoudal G, Ankri N, Debanne D. Long-term enhancement of neuronal excitability and temporal fidelity mediated by metabotropic glutamate receptor subtype 5. J Neurosci 2003;23:10238–10248. [PubMed: 14614082]

Svirskis G, Dodla R, Rinzel J. Subthreshold outward currents enhance temporal integration in auditory neurons. Biol Cybern 2003;89:333–340. [PubMed: 14669013]

Svirskis G, Kotak V, Sanes DH, Rinzel J. Enhancement of signal-to-noise ratio and phase locking for small inputs by a low-threshold outward current in auditory neurons. J Neurosci 2002;22:11019–11025. [PubMed: 12486197]

Svirskis G, Kotak V, Sanes DH, Rinzel J. Sodium along with low-threshold potassium currents enhance coincidence detection of subthreshold noisy signals in MSO neurons. Journal of neurophysiology 2004;91:2465–2473. [PubMed: 14749317]

Trussell LO. Synaptic mechanisms for coding timing in auditory neurons. Annu Rev Physiol 1999;61:477–496. [PubMed: 10099698]

Tzounopoulos T, Kim Y, Oertel D, Trussell LO. Cell-specific, spike timing-dependent plasticities in the dorsal cochlear nucleus. Nat Neurosci 2004;7:719–725. [PubMed: 15208632]

Voigt HF, Young ED. Neural correlations in the dorsal cochlear nucleus: pairs of units with similar response properties. Journal of neurophysiology 1988;59:1014–1032. [PubMed: 3367194]

White JA, Young ED, Manis PB. The electrotonic structure of regular-spiking neurons in the ventral cochlear nucleus may determine their response properties. Journal of neurophysiology 1994;71:1774–1786. [PubMed: 8064348]

Zhang S, Oertel D. Neuronal circuits associated with the output of the dorsal cochlear nucleus through fusiform cells. Journal of neurophysiology 1994;71:914–930. [PubMed: 8201432]

Zhao HB, Liang ZA. Processing of modulation frequency in the dorsal cochlear nucleus of the guinea pig: amplitude modulated tones. Hear Res 1995;82:244–256. [PubMed: 7775289]

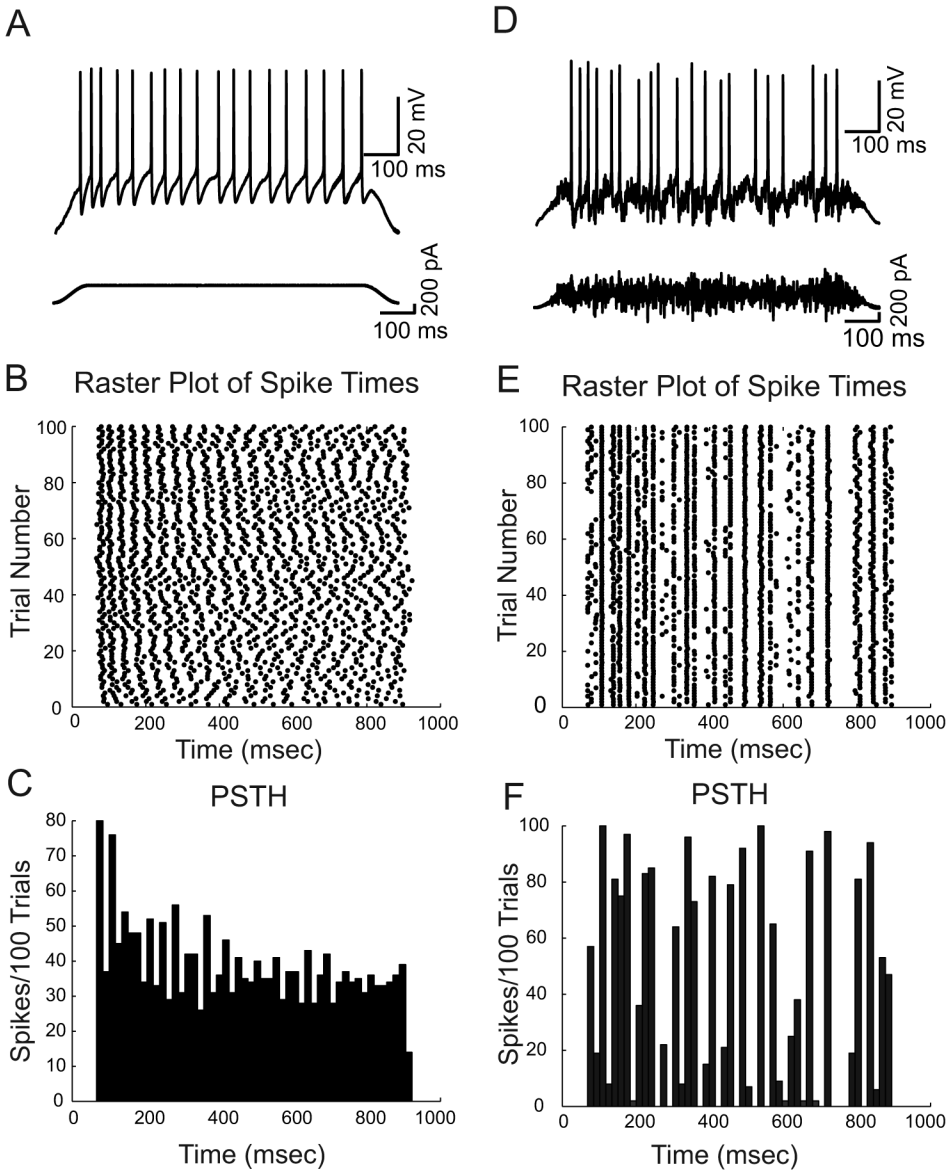

Figure 1.

Spike trains produced by noisy currents show repeatable structure, whereas spike trains produced by flag current steps are not repeatable. **A.** Raw traces of spike trains resulting from a flat current pulse, showing regular firing. The peak-to-peak current amplitude is 500 pA. **B.** Raster plots of spike times over 100 trials for the cell shown in A. Although the cell is regular, the spike times are not reproducible with respect to the onset of the stimulus. **C.** PSTH showing rate adaptation and weak “chopping” due to discharge regularity. **D.** Response of cell in A to the same current pulse with superimposed noise. The firing is less regular. **E**. Rasterplot, as in B, for noise response. Note that there are discrete events in the firing pattern that are reproducible across trials. **F**. PSTH for data in E. Clustered spike times produce a PSTH with large moment-to-moment changes in rate. PSTH bin width in C and E is 10 msec.

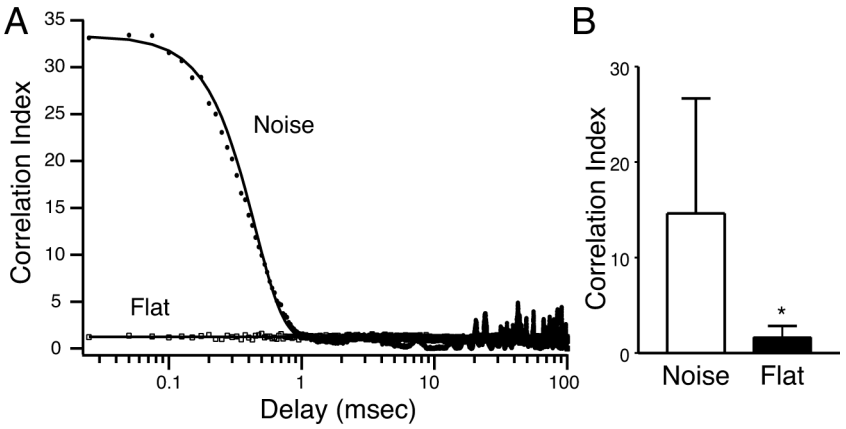

Figure 2.

Measurement of spike timing across trials using the shuffled autocorrelation method. **A** SAC for the same cell as in figure 1 and 2. The open squares denote the delay times for flat currents, and the filled circles denote delay times for the noisy currents. Gaussian fits are shown as lines. The abcissa is on a log scale to emphasize the correlation for delays less than 1 msec. A value of 1 is expected for a random process, or spike timing that is uncorrelated across trials. **B** Pooled data comparing CI for 45 cells. The noisy CI is significantly larger than the flat CI ($P<0.001$, paired t-test; mean difference=13.0).

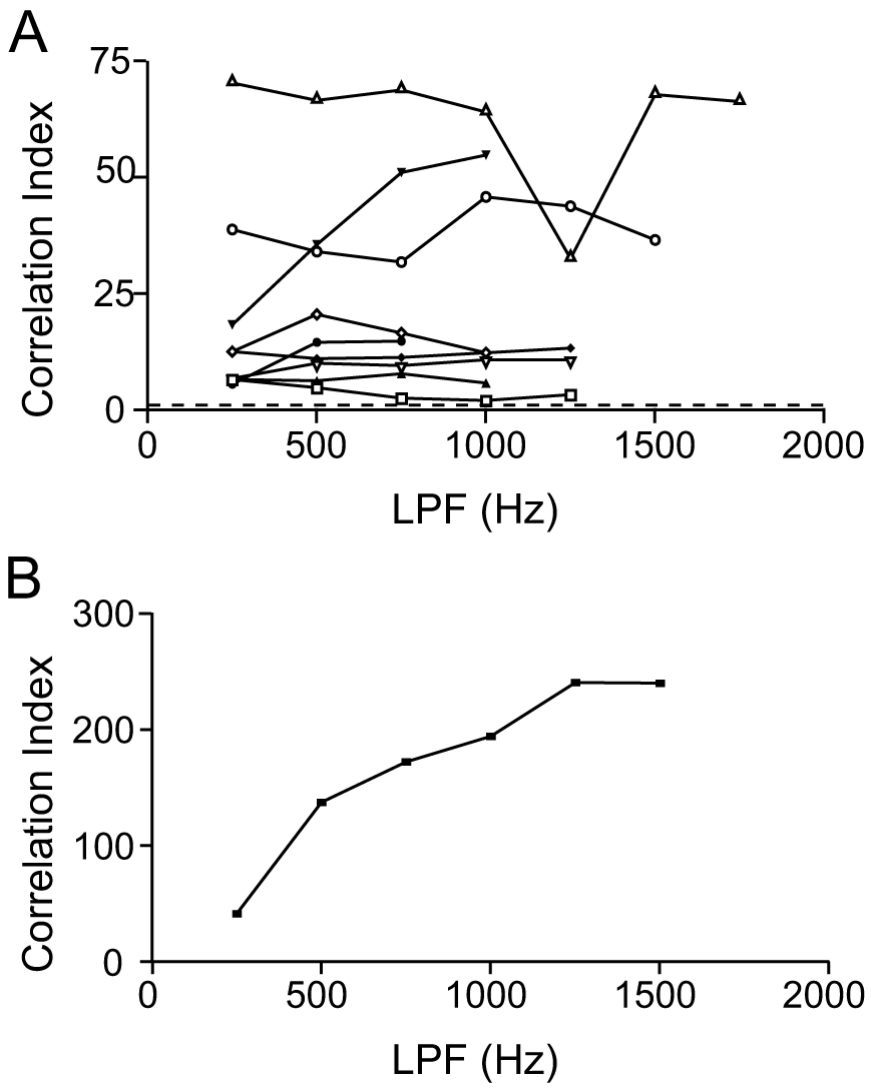

Figure 3.

The frequency content of the noisy current does not affect the ability of the cells to fire precisely. **A, B** CI is plotted as a function of the cutoff frequency of a low-pass filter applied to the noise stimulus. Each line represents a separate cell (N=10; cell in B is on a different ordinate scale).

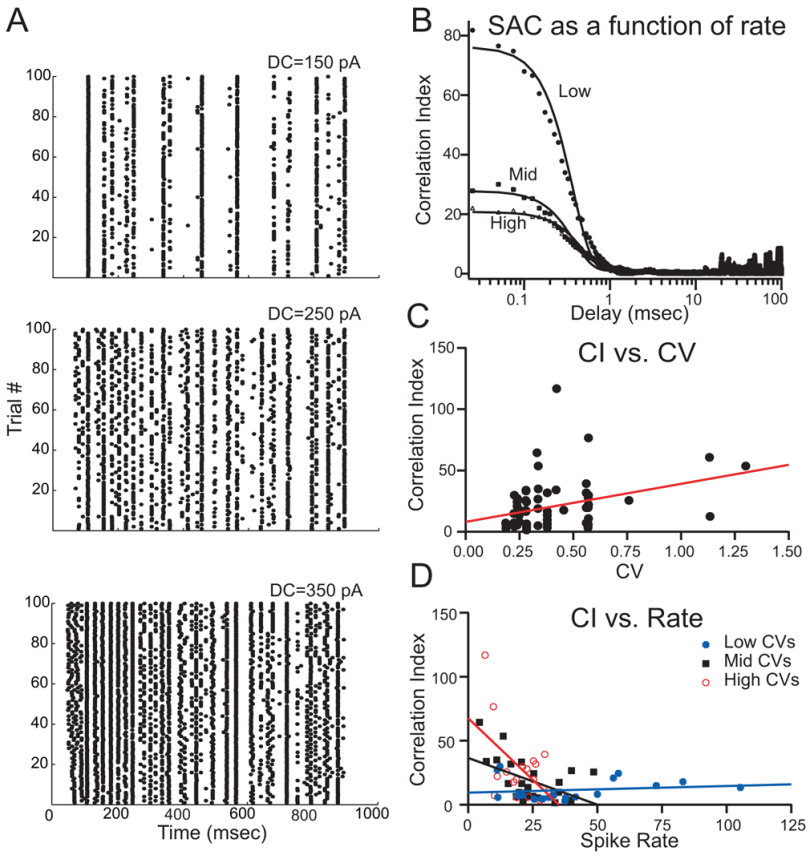

Figure 4.

Mean firing rate affects spike timing and reliability. **A**. Raster plots are shown for a single cell firing at different rates (upper plot is 9.8 spikes/second, middle plot is 16.6 spikes/second, lower plot is 25.4 spikes/second). **B**. SACs computed from data in A. Filled circles denote delays for low rate, filled squares denote medium rate, and triangles denote high rate. The SACs are fitted by a Gaussian function, as in Figure 4. **C**. Scatterplot of CI with the stimulus variance, CV_s , for 26 cells driven at different rates. The CI and CV_s are positively correlated. **D** Scatterplot of CI and spike rate, grouped by CV_s. Low (gray circles); intermediate, (black squares); high, (open circles). The correlation between CI and spike rate was significant for cells where the CV_s was at high or intermediate ranges ($R=0.2513$, $P<0.05$ for high; $R=0.1838$, $P<0.05$ for intermediate).

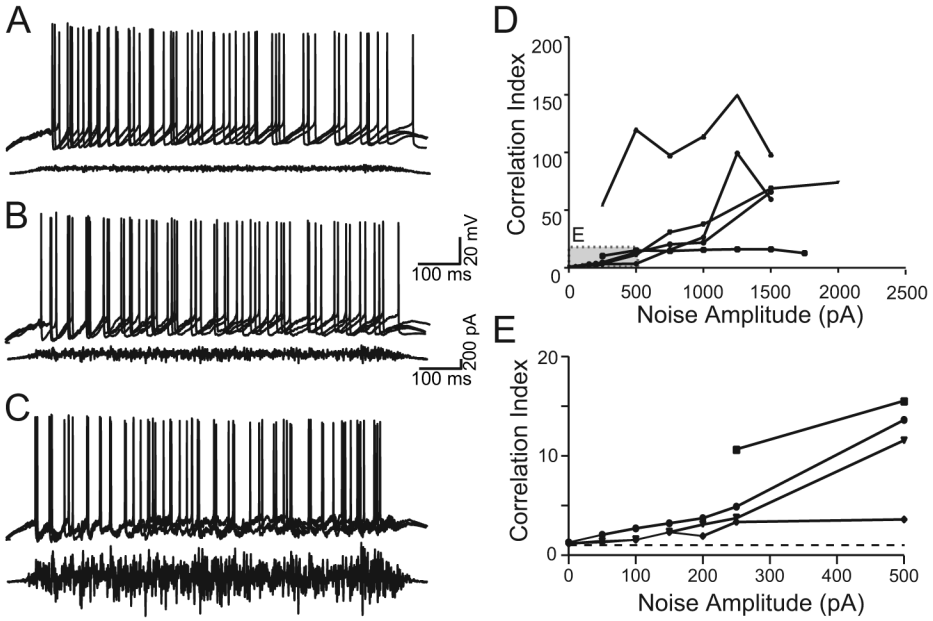

Figure 5.

Increasing the noise amplitude increases spike timing precision. **A-C** Traces from 5 consecutive trials, overlaid to show spikes elicited in response to a noise stimulus with low (A), middle (B), or high (C) amplitude. All data from the same cell. **D** Increaseing the noise amplitude increases the CI. Each line is a separate cell. **E** The gray box near the origin in D is expanded to show increases with small amounts of noise. Dashed line, CI = 1.

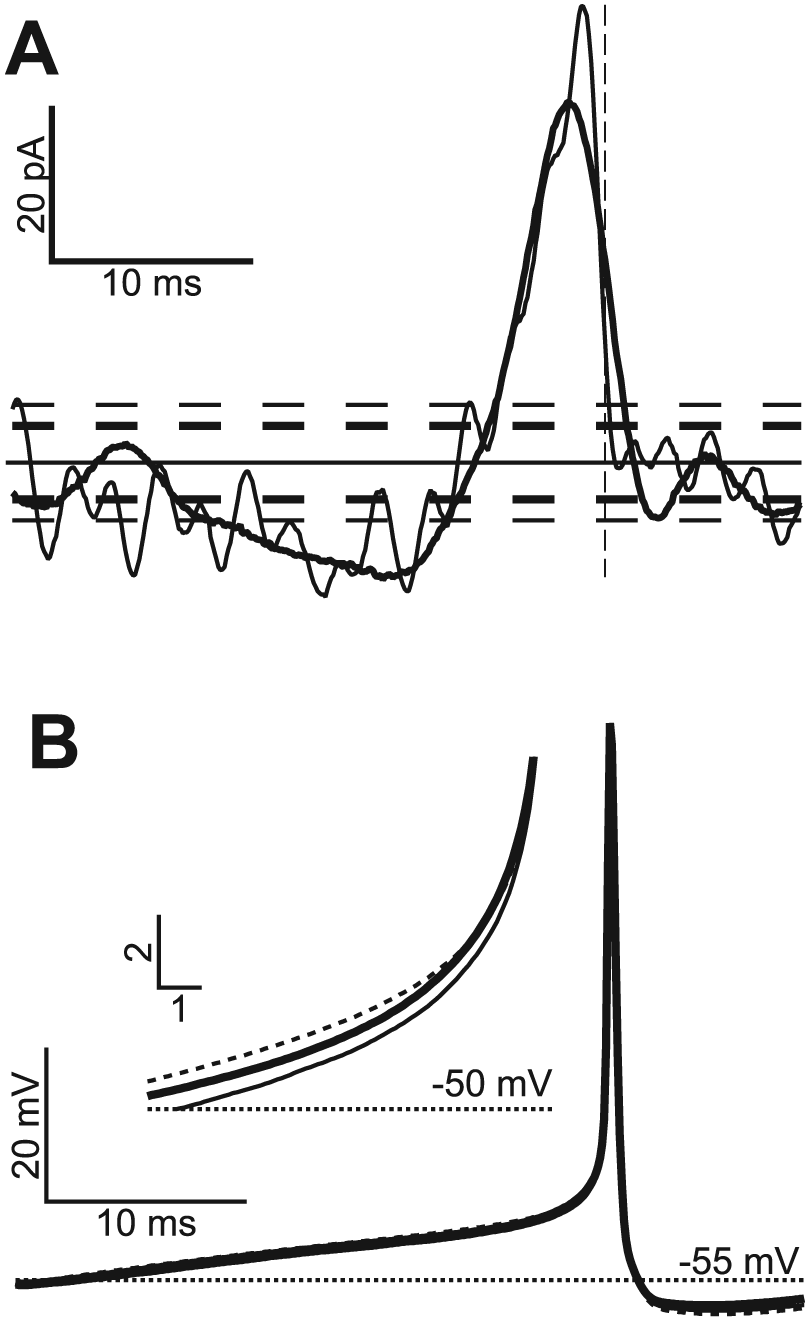

Figure 6.

Typical spike triggered average. **A** The spike triggered average current before and during an action potential is shown for noisy currents filtered at 250 Hz (thick line), or 500 Hz (thin line). Calculated 95%-5% confidence intervals are shown as dashed lines. The vertical dashed line corresponds to the peak of the action potential. **B** Action potential shape for flat, 250 Hz, and 500 Hz low-pass filtered noise. There is little variation in action potential shape. The inset shows the small variations in membrane potential leading up to the action potential around threshold. Inset calibration is in ms and mV.

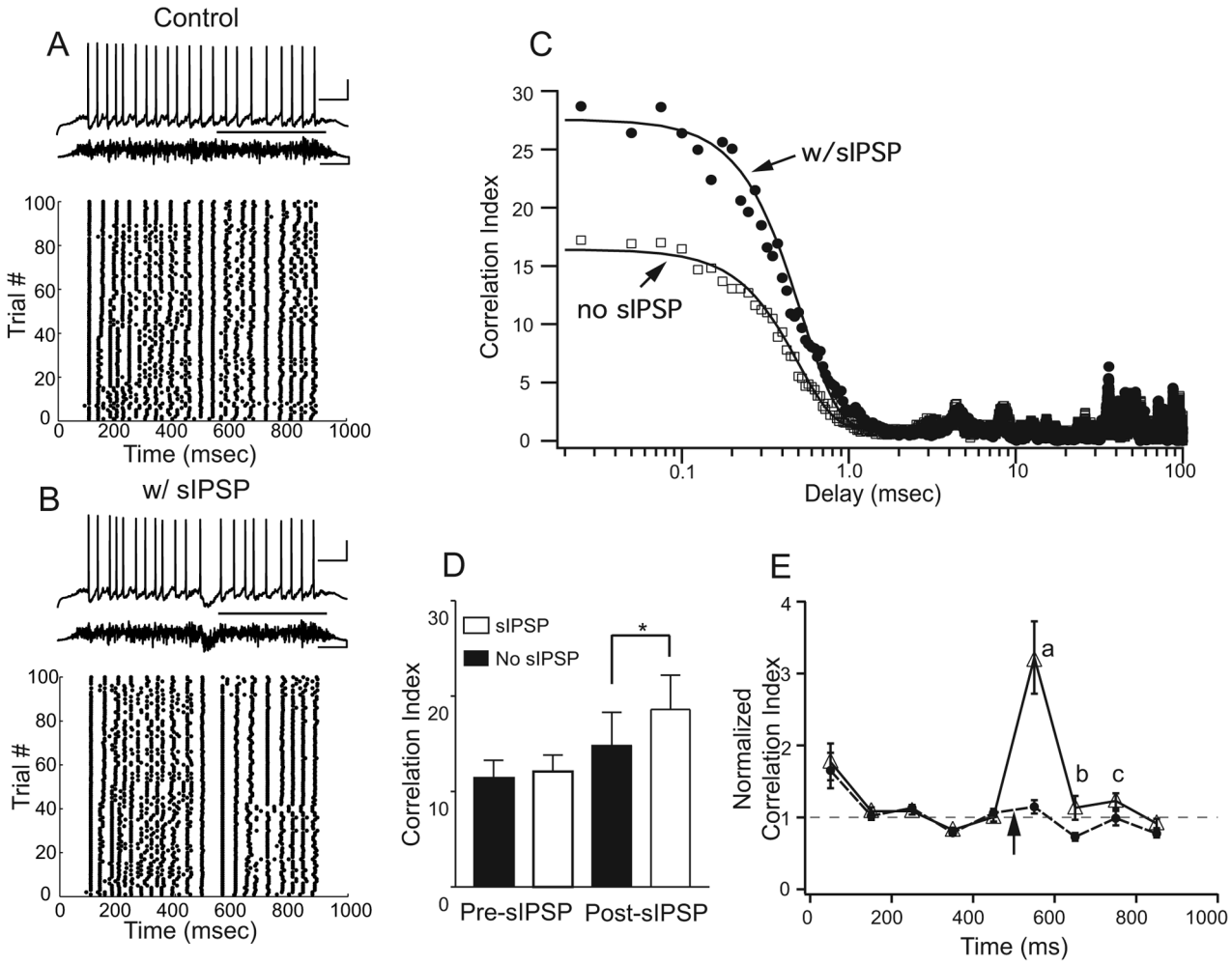

Figure 7.

A brief hyperpolarization (simulated IPSP) can improve subsequent spike timing. **A,B** Single traces and raster plots for spike trains from a single cell when presented with a noise pulse that either did not (A) or did (B) include a sIPSP 500 msec after the start of the pulse. Scale bars: Voltage, 20mV and 100 msec; Current, 200 pA and 100 msec. **C** SAC computed for spike times during the last 500 msec of the stimulus. Delay values for spike times when the stimulus included a sIPSP are shown by the filled circles. Delay values for spike times when the stimulus did not contain a sIPSP are shown in open squares. The points have been fit with Gaussians (lines). The sIPSP increases spike reliability. **D** Summary comparison of CI before and after the sIPSP. Pre-IPSP denotes the spike times that occurred in the first 500 msec of the stimulus. Post-sIPSP denotes the spike times that occurred in the last 500 msec of the stimulus. CI was significantly greater for spike times that occurred after a sIPSP was imposed upon the stimulus ($P<0.001$, $N = 31$, paired t-test). **E** CI calculated with a sliding 100-msec time window shows that the largest change occurs in the first 100 msec after an sIPSP (point a), but the CI is still significantly elevated ($P <0.001$, $N = 31$, paired t-test) out to 300 msec after the sIPSP (b,c).

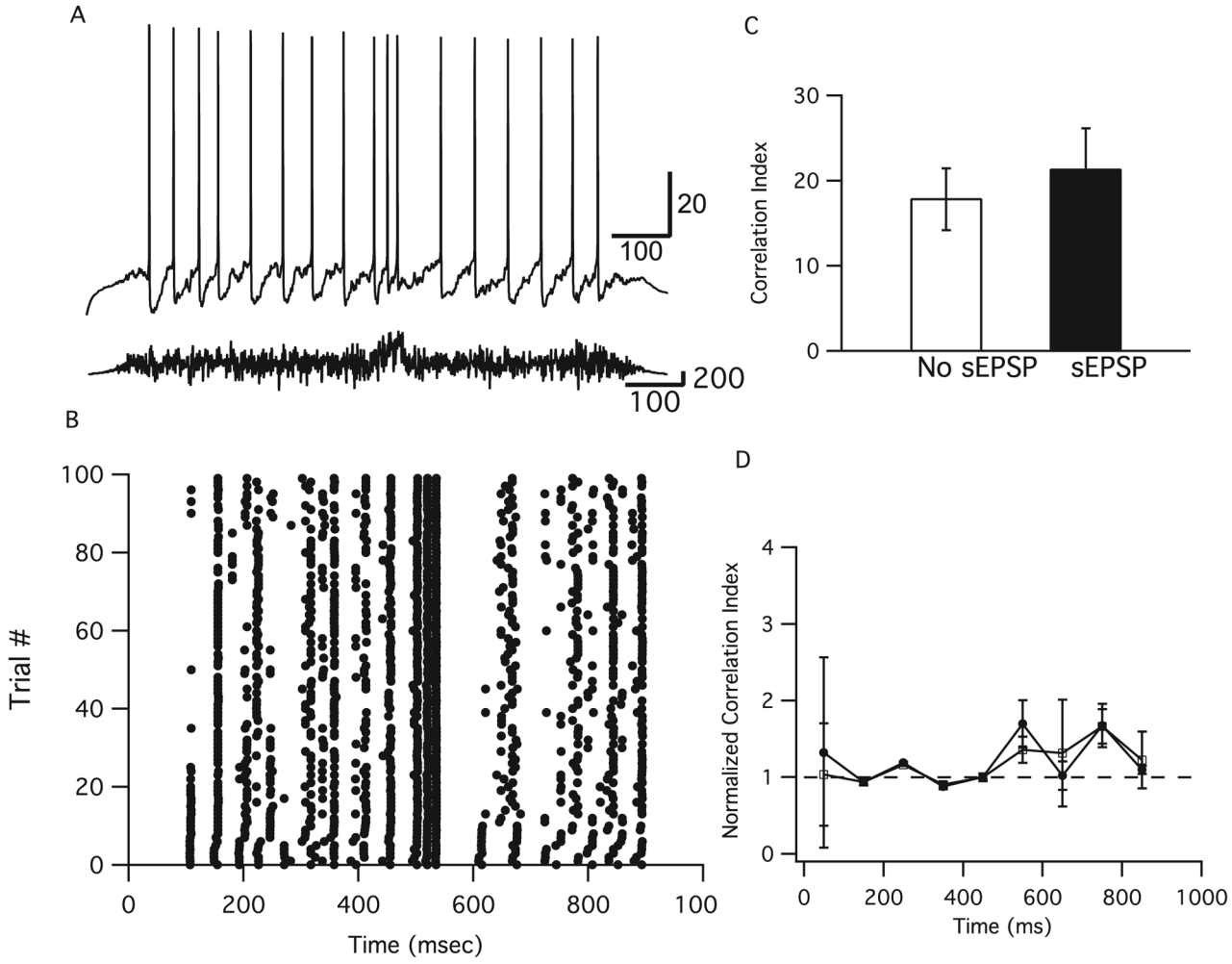

Figure 8.

Depolarizing events, such as a simulated sEPSP, can also improve spike timing. **A** Raw voltage and current traces for a cell stimulated with an sEPSP at 500 msec lateny. **B** Raster plot of spikes for the same cell as in A, where the stimulus contained an sEPSP. **C** Group data shows that the CI of spike times increased when a sEPSP was added to the stimulus ($P<0.05$, $N=13$, paired t-test). **C** CI calculated with a sliding 100-msec time window shows that there are no significant differences in spike times from stimuli with or without a sEPSP.

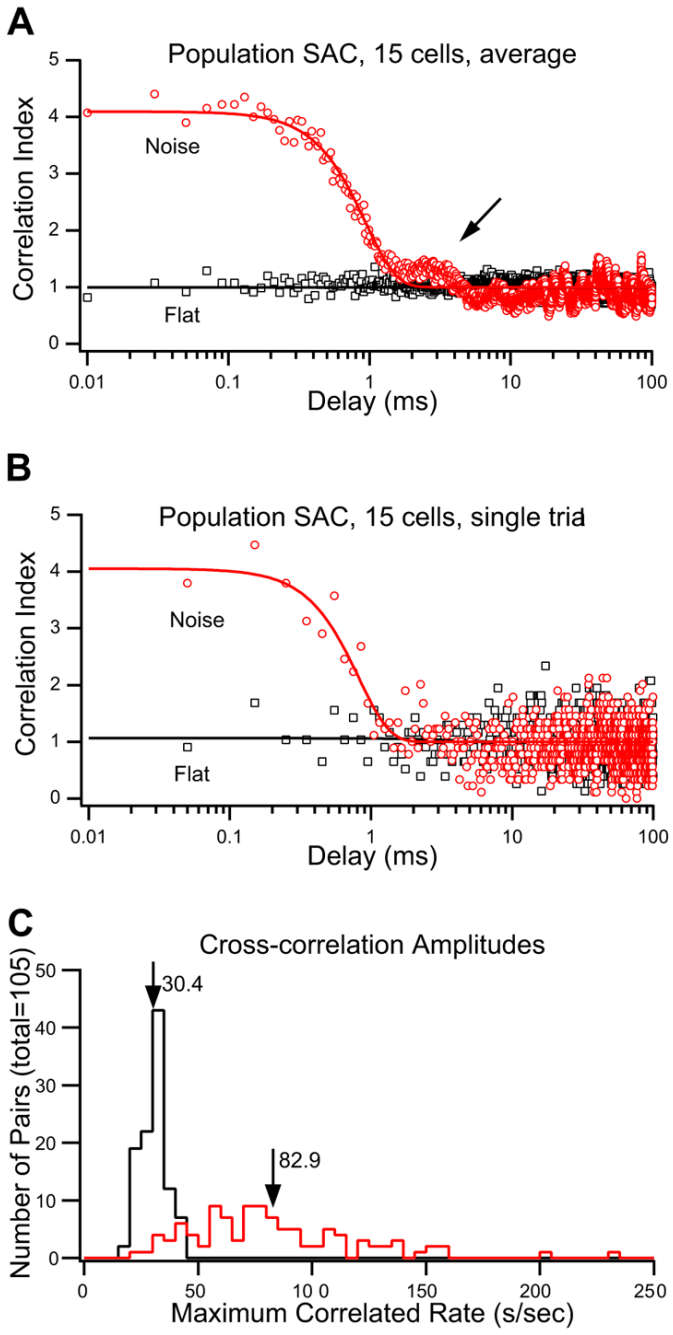

Figure 9.

Different cells can synchronize to common features in the stimulus. The SAC was computed across a population of 15 cells recorded from 6 separate preparations in response to the same frozen noise stimulus (Gaussian noise, low-pass filtered at 500 Hz). **A** A central mound is evident in response to the noise stimulus, indicating that the average rate increases by about four-fold in response to suprathreshold inputs. Note the narrow central peak (half-width, 0.84 msec). Flat current pulses, despite generating regular firing, do not lead to synchronized activity (open squares). Solid lines are fits of a Gaussian function to the data. Average of 100 trials. **B** SAC for a single 1-second trial shows a similar shape to the average, indicating detectable synchrony in a single trial.. **C** Summary of the peak cross-correlation rates across the 105

possible pair-wise combinations for the 15 cells analyzed in A and B. The black histogram shows the peak correlation rates for flat stimuli; these are not significantly different than the average firing rates of the cell pairs. The red histogram shows the peak correlation rates for noisy stimuli. Arrows indicate the mean rates for the two histograms. The mean correlation rate for noisy stimuli is 2.7 times the flat rate.